The $^{18}F(p,\alpha)\ ^{15}O$ low-energy S–factor: A microscopic approach

M. Dufour, P. Descouvemont

The ^{18}F(p,α)^{15}O low-energy S-factor: a microscopic approach

M. Dufour

IReS Bat27, IN2P3-CNRS/Université Louis Pasteur BP28, F-67037 Strasbourg Cedex 2 - France

P. Descouvemont [1]

Physique Nucléaire Théorique et Physique Mathématique, CP229 Université Libre de Bruxelles, B1050 Brussels, Belgium

Abstract

The ^{18}F(p,α)^{15}O S-factor is determined in a microscopic cluster model. The wave functions are defined in the Generator Coordinate Method, involving various ^{18}F+p, ^{15}O+α, and ^{18}Ne+n configurations. We analyze the ^{19}Ne level scheme, and test the model with the ^{19}F spectrum, better known experimentally. We focus on $1/2^+$ and $3/2^+$ states, corresponding to s waves, and expected to represent the main contribution in the ^{18}F(p,α)^{15}O cross section at stellar energies. The $1/2^+$ partial wave is shown to play an important role in a wide energy range. This property reduces the uncertainties associated with interference patterns in the $3/2^+$ contribution. The relevant $1/2^+$ states have been observed in ^{19}F, but have not been searched for in ^{19}Ne. An elastic-scattering experiment above 1 MeV is suggested.

1 Introduction

Information about the nucleosynthesis and the ejection mechanism in novae can be essentially deduced from gamma-ray emission originating from electron-positron annihilations at 511 keV following the β^+ decay of ^{18}F. A precise interpretation of the measurements performed by γ-astronomy detectors relies on an accurate knowledge of the destruction modes of ^{18}F in novae. In this context, ^{18}F(p,α)^{15}O is believed to be the most relevant reaction [1,2].

[1] Directeur de Recherches FNRS

The typical temperature range in novae is of the order of $(1-4) \times 10^8$ K. Consequently, ^{19}Ne resonances relevant in the burning process are located in an interval of about 1 MeV above the ^{18}F+p threshold ($Q = 6.41$ MeV) [1,3]. Many uncertainties remain on the determination of the ^{18}F(p,α)^{15}O reaction rate at these energies. Until now, the astrophysical S-factor has been essentially calculated as a sum of contributions of individual states (see, however, Ref. [4], where interference effects are discussed). Among those resonances, only two of them seem to be reasonably well understood. A $3/2^+$ state at $E_x = 7.07$ MeV ($E_{cm} = 0.66$ MeV) is an s wave, and is known to be a single particle state, with a large spectroscopic factor [5,6]. It has been widely investigated in the literature, through transfer [7–9] or elastic [10,11] reactions, or with indirect methods [12–18]. On the other hand, the existence of a $3/2^-$ state at $E_{cm} = 0.33$ MeV [14] is now well established but, owing to its p-wave nature, plays a role in a limited temperature range only.

Some experiments focus on the ^{19}F mirror nucleus, and derive ^{19}Ne properties by assuming charge symmetry on the reduced widths and spectroscopic factors. In this case, in addition to the experimental difficulties inherent to each technique, a theoretical uncertainty may arise from the use of charge symmetry. The Q values in both nuclei are quite different and Coulomb effects are expected to be non-negligible.

This paper is devoted to a microscopic study of the ^{18}F(p,α)^{15}O reaction at stellar energies. The theoretical framework combines a large-scale variational basis (Extended Two Cluster Model - ETCM) and a new interaction (Extended Volkov Interaction - EVI) (see Refs. [19,20] and references therein). Microscopic cluster models [21] are known to be well adapted to the description of reactions relevant in astrophysics, which involve low-energy cross sections and radioactive nuclei. Antisymmetrization between all nucleons, center-of-mass motion, good quantum numbers and boundary conditions are exactly treated. Bound, resonant and scattering states of the system are described in a unified way through the microscopic R-Matrix method [22] allowing a direct calculation of radiative-capture and transfer cross sections. Furthermore the small number of parameters involved gives them a significant predictive power.

Previously, the same model has been successfully applied to the study of the ^{13}C(α,n)^{16}O transfer reaction [20]. The ETCM provides a large variational space and the EVI improves the hamiltonian by introducing an additional degree of freedom. In the case of transfer reactions, the threshold between the entrance and exit channels and another important property such as the location of a state can be then reproduced simultaneously.

In order to describe the ^{18}F(p,α)^{15}O reaction, the ETCM wave functions of ^{19}Ne are defined as a sum of ^{18}F+p, ^{15}O+α and ^{18}Ne+n two-cluster basis func-

tions. The ^{18}F, ^{18}Ne, and ^{15}O nuclei are described by clusters involving major s, p and sd harmonic oscillator shells. Consequently, the GCM wave function is expanded over many channels. The large variational basis obtained in this way is expected to provide a good description of the asymptotic conditions of the reaction and of some resonances relevant in the ^{18}F(p,α)^{15}O cross section.

Of course the applicability of microscopic models is essentially limited by the level density. In the present case, owing to the large Q value, and to the low isospin, the level density near threshold is significant (typically a few levels per MeV). Consequently a microscopic approach cannot be expected to reproduce all relevant resonances. The present work is more an exploring study of the reaction than an exhaustive review of resonance properties. We essentially focus on the $1/2^+$ and $3/2^+$ states, which correspond to the s waves in the ^{18}F+p motion.

In Section 2, we briefly present the model, and emphasize the definition of the spectroscopic factors. Charge symmetry effects are analyzed in Section 3, before the analysis of the ^{18}F(p,α)^{15}O S factor. Concluding remarks are given in Section 4.

2 The microscopic model

2.1 Wave functions

The wave functions are defined in the Generator Coordinate Method (GCM) which assumes a cluster structure for the A-nucleon system [21]. In a given partial wave $JM\pi$, the wave function of the system is given by a superposition of ^{18}F+p, ^{15}O+α and ^{18}Ne+n cluster wave functions, each channel involving various excited states (see Ref. [19] for details). More precisely the wave function is given by

$$\Psi^{JM\pi} = \sum_i \Psi^{JM\pi}_{^{18}F(i)+p} + \sum_j \Psi^{JM\pi}_{^{15}O(j)+\alpha} + \sum_k \Psi^{JM\pi}_{^{18}Ne(k)+n}, \quad (1)$$

where the sums run over all internal states. The ^{18}F and ^{18}Ne wave functions are defined in the sd shell model with all configurations allowed by the Pauli principle. For ^{15}O, we use a closed p shell with one hole. This procedure provides various states which are presented in Table 1.

In a two-cluster theory, each component of Eq. (1) is written as

Table 1
Shell-model states included in the two-cluster GCM basis. The bracketed values correspond to the number of states for a given spin.

Nucleus	States
^{18}F	0^+ (3), 1^+ (7), 2^+ (8), 3^+ (6), 4^+ (3), 5^+ (1)
^{18}Ne /^{18}O	0^+ (3), 1^+ (2), 2^+ (5), 3^+ (2), 4^+ (2)
^{15}O /^{15}N	$1/2^-$(1), $3/2^-$(1)

$$\Psi_\alpha^{JM\pi} = \sum_{\ell I} \mathcal{A}\left[Y_\ell(\Omega_\rho) \otimes [\phi_1^{I_1\pi_1} \otimes \phi_2^{I_2\pi_2}]^I\right]^{JM} g_{\alpha\ell I}^{J\pi}(\rho), \tag{2}$$

where (I_1, I_2) are the spin of the colliding nuclei in channel α (α refers to the partition and to the excitation level), I is the channel spin, and ℓ the relative angular momentum. In Eq. (2), $g_{\alpha\ell I}^{J\pi}(\rho)$ is the radial function depending on the relative coordinate ρ, and $\mathcal{A}$ is the antisymmetrization operator. In the GCM, these radial wave functions are expanded over displaced gaussian functions, which makes Eq. (2) equivalent to a combination of projected Slater determinants, well adapted to numerical calculations. The gaussian basis functions are centered at different locations called the generator coordinates (see Ref. [21] for more information). In the GCM, the asymptotic behaviour of the wave function (2) is of course gaussian. This is corrected by the microscopic R-matrix method [22] which restores the coulombian dependence of the wave function.

A key issue in the treatment of transfer reactions is the threshold problem. When the internal wave functions and the nucleon-nucleon interaction are chosen, the model is parameter free, and the thresholds are an output of the theory. We have recently developed a new nucleon-nucleon interaction [19] based on the Volkov force, but with more flexibility. This force allows to constrain a threshold, and to keep one parameter to reproduce some important property of the system, such as the energy of a resonance. The choice of the interaction will be specified in Section 3. The ^{18}F and ^{18}Ne/^{18}O energy spectra have been already discussed in Ref. [19]. Although the interaction adopted here is slightly different, the present spectra are very similar to those of Ref. [19].

2.2 Spectroscopic factors

In a microscopic cluster model, the radial wave functions $g_{\alpha\ell I}^{J\pi}(\rho)$ can be transformed as

$$\tilde{g}_{\alpha\ell I}^{J\pi}(\rho) = \sum_{\alpha'\ell' I'} \int \mathcal{N}_{\alpha\ell I,\alpha'\ell' I'}^{J\pi}(\rho,\rho') g_{\alpha'\ell' I'}^{J\pi}(\rho') d\rho', \tag{3}$$

where $\mathcal{N}^{J\pi}(\rho,\rho')$ is the overlap kernel [23,24], which is computed numerically according to the method proposed by Varga and Lovas [25]. From these functions, we derive the spectroscopic factors in a given $(\alpha\ell I)$ channel by

$$\mathcal{S}^{J\pi}_{\alpha\ell I} = \int_0^\infty \left(\tilde{g}^{J\pi}_{\alpha\ell I}(\rho)\right)^2 \rho^2 d\rho. \tag{4}$$

The spectroscopic factor measures the contribution of a given channel in a many-body wave function. A large value indicates a dominant cluster structure in this channel. Notice that, in most experimental works, the spectroscopic factor is based on simple potential-model wave functions. Physical solutions (in DWBA expressions, for example) are approximated by

$$\tilde{g}^{J\pi}_{\alpha\ell I}(\rho) \approx \mathcal{S}^{pot}_{\alpha\ell I}\ g^{J\pi}_{pot}(\rho), \tag{5}$$

where $g^{J\pi}_{pot}(\rho)$ is derived from some potential. In addition to uncertainties related to the choice of the potential, the definition itself of the spectroscopic factor is different. Although both approaches should provide qualitatively consistent results, a precise comparison is often difficult (see, for example, Ref. [26]).

3 Application to ^{18}F(p,α)^{15}O and to the ^{19}Ne spectroscopy

3.1 Conditions of the calculation

As mentioned previously, the GCM basis functions involve ^{18}F+p, ^{18}Ne+n and ^{15}O+α (or mirror) configurations with, for each heavy nucleus, several excited states. In the treatment of transfer reactions, reproducing the Q value is a key issue, and we use the EVI [19] complemented by a zero-range spin-orbit interaction [27,19] with the amplitude S_0 as free parameter. The three parameters of the interaction are determined as follows: S_0 is fitted on the ^{15}O$(3/2^-)-^{15}$O$(1/2^-)$ experimental energy ($S_0 = 28$ MeV.fm^5); the remaining parameters are fitted on the ^{18}F(p,α)^{15}O experimental threshold, and on the energy of the $3/2^+$ resonance in ^{19}Ne ($E_x = 7.07$ MeV, $E_{cm} = 0.66$ MeV) which is known to be a single-particle state [5], accurately described by a ^{18}F+p model. This provides $W = 0.7661,\ M = 0.2339,\ B = -0.52,\ H = 0.52$ as EVI parameters.

The oscillator parameter, common to all clusters, is chosen as $b = 1.6$ fm, which represents a compromise between their r.m.s. radii and their binding

energies. The generator coordinates are taken from $R = 2.4$ fm to $R = 10.8$ fm with a constant step of 1.4 fm. In the R-matrix calculations, we use a channel radius $a = 10.1$ fm. Large values are necessary to make sure that antisymmetrization effects and nuclear contributions between the clusters are negligible, as required by the R-matrix method. As soon as these conditions are satisfied, the physical results do not depend on the channel radius.

3.2 Discussion of Coulomb effects

The use of charge symmetry is widely used in the literature to deduce spectroscopic properties of ^{19}Ne states from the mirror nucleus ^{19}F. Here we want to address two important issues: (*i*) a test of the ability of the GCM to account for Coulomb shifts; this is done on low-lying states where the level scheme of both nuclei is firmly established. (*ii*) To compute reduced widths and spectroscopic factors of ^{19}Ne and ^{19}F; as the model includes the Coulomb force exactly, this will test the accuracy of the charge-symmetry assumption on these quantities. This assumption is used in indirect methods, where the measurements deal with spectroscopic information on the ^{19}F nucleus.

Concerning item (*i*), we have readjusted the nucleon-nucleon interaction individually for well known ^{19}F positive-parity low-lying states of ^{19}F. Then the theoretical ^{19}Ne energy is determined with the same nuclear interaction. This allows to quantify the precision of the method to deduce ^{19}Ne energies. The results are given in Table 2, which shows that the difference between theory and experiment is at most 0.14 MeV. It is reasonable to assume that a similar accuracy can be expected for more excited states, near the proton threshold.

Table 2
^{19}Ne energies (in MeV) after tuning of the interaction on ^{19}F levels (see text).

J^π	^{19}F (exp)	^{19}Ne (exp)	^{19}Ne (GCM)
$1/2^+$	-10.42	-6.41	-6.27
$5/2^+$	-10.24	-6.17	-6.13
$3/2^+$	-8.88	-4.87	-4.73
$7/2^+$	-6.05	-2.03	-2.07

Let us now discuss spectroscopic factors and reduced widths. We consider here $1/2^+$ and $3/2^+$ states, as mentioned previously. In each case, we have a strongly bound state, a resonance, and a state located near threshold. In Table 3, we present the spectroscopic factors in various channels. The low-lying $1/2^+$ and $3/2^+$ states have similar spectroscopic factors in the three

partitions. This is not surprising in an antisymmetric model: for compact states, different configurations may describe equally well the wave function. For ^{19}F, the spectroscopic factors in the proton channel are in qualitative agreement with the values of Iliadis and Wiescher [26] obtained in various models. The second GCM levels correspond to α cluster states, well known in cluster theories [28,29], and characterized by large α spectroscopic factors.

As expected [5], the 7.07 MeV state in ^{19}Ne presents a large spectroscopic factor in the proton channel. Note however that the theoretical definition of the spectroscopic factor (4) might give slightly different results from the method based on the potential model. This was already pointed out by Iliadis and Wiescher [26] who compare spectroscopic factors deduced from the shell model, from DWBA analysis, and from the potential model. Using a Woods-Saxon potential, Fortune and Sherr [5,6] recommend slightly lower values ($\mathcal{S}_p(0) = 0.49 \pm 0.03$), but the single-particle character of this resonance is confirmed by the GCM. A $1/2^+$ state presents the same properties, and is expected to have some influence on the ^{18}F(p,α)^{15}O S factor.

Concerning charge symmetry, the GCM shows that the spectroscopic factors in ^{19}F and ^{19}Ne are very close to each other, even in less important configurations. This supports the assumption of charge symmetry in DWBA analyses (see for example [15]).

Table 3
Proton, neutron and α spectroscopic factors for the first three GCM states in ^{19}F and ^{19}Ne. The ℓ values are given in brackets. Energies E_x (in MeV) correspond to the experimental values.

	^{19}F ($J = 1/2^+$)					^{19}Ne ($J = 1/2^+$)				
State	E_x	$\mathcal{S}_n(0)$	$\mathcal{S}_n(2)$	$\mathcal{S}_p(0)$	$\mathcal{S}_\alpha(1)$	E_x	$\mathcal{S}_p(0)$	$\mathcal{S}_p(2)$	$\mathcal{S}_n(0)$	$\mathcal{S}_\alpha(1)$
1	0	0.156	0.009	0.198	0.165	0	0.173	0.010	0.183	0.159
2	5.94	0.045	0.003	0.008	0.806		0.082	0.003	0.003	0.768
3	8.65	0.456	0.002	0.195	0.084		0.707	0.000	0.103	0.094
	^{19}F ($J = 3/2^+$)					^{19}Ne ($J = 3/2^+$)				
State	E_x	$\mathcal{S}_n(0)$	$\mathcal{S}_n(2)$	$\mathcal{S}_p(2)$	$\mathcal{S}_\alpha(1)$	E_x	$\mathcal{S}_p(0)$	$\mathcal{S}_p(2)$	$\mathcal{S}_n(2)$	$\mathcal{S}_\alpha(1)$
1	1.55	0.029	0.318	0.095	0.159	1.54	0.035	0.352	0.087	0.149
2	5.50	0.016	0.456	0.000	0.543		0.024	0.505	0.001	0.476
3		0.772	0.073	0.010	0.021	7.07	0.874	0.129	0.001	0.006

Reduced widths are presented in Table 4. They are calculated at the R-matrix

channel $a = 10.1$ fm. Reduced widths represent a useful complement to spectroscopic factors: up to a simple factor, they provide the wave function evaluated at $\rho = a$. Conversely, the spectroscopic factors are obtained from an integral of the wave functions over the whole space. We therefore expect that charge symmetry is less good in reduced widths as, by definition of the R matrix channel, the interaction is dominated by the Coulomb force. This property is confirmed by the results displayed in Table 4. Charge symmetry is a rather poor approximation for reduced widths. This result arises from two reasons: of course the nuclear charges are different, but the Q values in ^{19}F and ^{19}Ne are also rather different ($Q_n = 10.42$ MeV in ^{19}F, and $Q_p = 6.41$ MeV in ^{19}Ne). At large distances, where the reduced widths are evaluated, the wave functions behave quite differently. The differences should decrease at larger channel radii, but the R-matrix requirements would not be satisfied. Our work therefore suggests that the charge-symmetry approximation should not be used for reduced widths.

Table 4
Proton, neutron and α reduced widths (at 10.1 fm) for the first three GCM states in ^{19}F and ^{19}Ne. Superscripts represent to the power of 10. All energies are expressed in MeV.

	^{19}F ($J = 1/2^+$)					^{19}Ne ($J = 1/2^+$)				
	E_x	$\gamma_n^2(0)$	$\gamma_n^2(2)$	$\gamma_p^2(0)$	$\gamma_\alpha^2(1)$	E_x	$\gamma_p^2(0)$	$\gamma_p^2(2)$	$\gamma_n^2(2)$	$\gamma_\alpha^2(1)$
1	0	6.31^{-5}	1.61^{-6}	5.88^{-5}	2.06^{-6}	0	1.91^{-4}	4.14^{-6}	2.46^{-5}	2.15^{-6}
2	5.94	1.48^{-4}	2.38^{-6}	2.05^{-6}	3.95^{-2}		1.95^{-3}	1.21^{-5}	4.44^{-7}	4.06^{-2}
3	8.65	8.26^{-3}	1.25^{-5}	1.77^{-3}	1.55^{-2}		9.20^{-2}	2.71^{-6}	1.46^{-4}	1.38^{-2}

	^{19}F ($J = 3/2^+$)					^{19}Ne ($J = 3/2^+$)				
	E_x	$\gamma_n^2(0)$	$\gamma_n^2(2)$	$\gamma_p^2(0)$	$\gamma_\alpha^2(1)$	E_x	$\gamma_p^2(0)$	$\gamma_p^2(2)$	$\gamma_n^2(2)$	$\gamma_\alpha^2(1)$
1	1.55	2.04^{-5}	5.13^{-5}	2.15^{-5}	1.06^{-5}	1.54	7.37^{-5}	1.61^{-4}	9.22^{-6}	1.10^{-5}
2	5.50	5.19^{-5}	2.56^{-4}	2.60^{-6}	1.62^{-2}		4.73^{-4}	1.21^{-3}	1.88^{-6}	1.39^{-2}
3		1.19^{-2}	2.32^{-4}	2.09^{-5}	3.51^{-3}	7.07	7.21^{-2}	1.05^{-3}	3.40^{-7}	1.06^{-3}

3.3 Spectroscopic properties of ^{19}F and ^{19}Ne

Our goal in this work is essentially to discuss the ^{18}F(p,α)^{15}O cross section, in the framework of a microscopic approach. We do not intend to discuss the level schemes in detail. Here we focus on two specific partial waves, $J = 1/2^+$ and $J = 3/2^+$, which correspond to s waves and which, consequently, are

expected to dominate the cross section at low energies. The level schemes are given in Figures 1 and 2, for $J = 1/2^+$ and $J = 3/2^+$, respectively.

Let us start with a discussion of Fig. 1, where we compare $1/2^+$ states derived from the GCM, and observed experimentally [3,12,16,18]. Energies are given from the ^{18}F+n and ^{18}F+p thresholds for ^{19}F and ^{19}Ne, respectively. Let us remind that the ^{18}F(p,α)^{15}O Q value and the $3/2^+$ (7.07 MeV) level in ^{19}Ne are fitted by the interaction, but that all other energies (thresholds, level energies) are determined without any fitting procedure. The ^{18}O+p threshold in ^{19}F is underestimated by the theory, but the ordering is correct. In ^{19}Ne, the ^{18}Ne+n threshold is located above 5 MeV, and is therefore not shown.

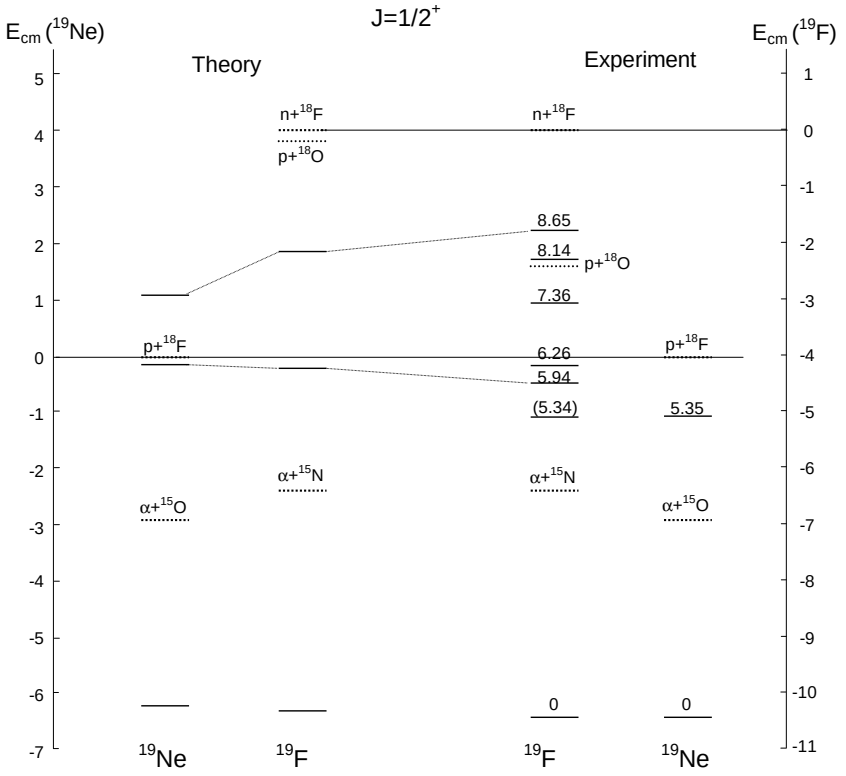

Fig. 1. ^{19}F and ^{19}Ne spectra for $J = 1/2^+$. All energies are in MeV. The thresholds are displayed as dotted lines. Experimental energies E_x are given.

The GCM energy of the ground states are in fair agreement with experiment (within 0.2 MeV). The spectroscopic factors in the p and α channels are similar (see Table 3). The second GCM $1/2^+$ state presents a dominant component in the 4+15 channel, as indicated by the large spectroscopic factors. Experimentally, the 5.94 MeV state in ^{19}F is known to be an α+^{15}N state, and has been discussed in previous single-channel α+^{15}N cluster models [28,29]. The GCM gives rise to a third $1/2^+$ resonance, at $E_x = 8.3$ MeV. Its width ($\Gamma_{GCM} = 180$ keV) suggests that the experimental counterpart is the 8.65 MeV

state ($\Gamma_{exp} \approx 300$ keV). The predicted energy is quite close to the experimental value.

The study of $1/2^+$ levels provides two conclusions:
(i) In ^{19}Ne, the third GCM level, analog of the 8.65 MeV state in ^{19}F, is located at lower energy, near 1 MeV above the ^{18}F+p threshold. Therefore it might play a role in the ^{18}F(p,α)^{15}O reaction. The large Coulomb shift is supported by the important spectroscopic factor (see Table 3). From theoretical arguments, this state can be considered as a single-particle state, similar to the $3/2^+$ (7.07 MeV) level in ^{19}Ne. Although it should play a role in the cross section, as s-wave resonance, it has not been identified yet in ^{19}Ne.
(ii) Comparing the theoretical and experimental ^{19}F spectra indicates that three levels are missing in the GCM. Although they are not observed in ^{19}Ne they might also contribute to the ^{18}F(p,α)^{15}O S-factor. As they are not described by the present two-cluster model, which includes many configurations, these states should have a more complicated structure, such as a three-body structure. It is consequently reasonable to assume that their spectroscopic factors in the p and α channels should be small, and that their role in the cross section should be of minor importance.

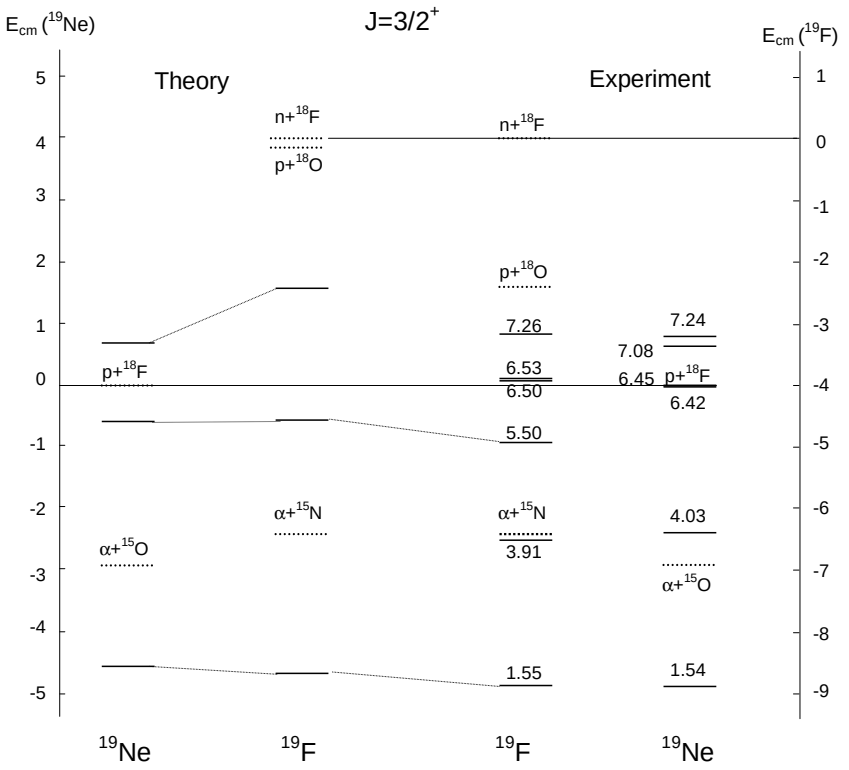

Fig. 2. ^{19}F and ^{19}Ne spectra for $J = 3/2^+$ (see caption to Fig. 1).

Let us now discuss $3/2^+$ states, displayed in Fig. 2. As for $J = 1/2^+$, they correspond to s waves. The nucleon-nucleon interaction has been fitted on

the energy of the 7.07 MeV resonance in ^{19}Ne, well known to be a single particle state, and hence well adapted to a ^{18}F+p model. Its proton and α widths are calculated as $\Gamma_p = 26$ keV, and $\Gamma_\alpha = 9$ keV. This provides a ratio $\Gamma_p/\Gamma = 0.74$ somewhat higher than experimentally, but the resonance strength $\omega\gamma = 4\Gamma_p\Gamma_\alpha/6\Gamma = 4.5$ keV is consistent with the data (see Ref. [9] for a review). As expected we find low-lying $3/2^+$ states, members of the $K = 1/2^+$ ground-state band in both nuclei. Without any fitting procedure the GCM energies are quite close to the experimental values. Table 3 shows that the ^{18}F+n (^{18}F+p) configuration is dominant, but the α channel also plays a role.

The second $3/2^+$ GCM state corresponds to an α-cluster molecular resonance, well known for many years [28,29]. As explained previously, the third GCM resonance is assigned to the 7.07 MeV state in ^{19}Ne. This state determines the ^{18}F(p,α)^{15}O S factor in a wide energy range. As pointed out by Fortune and Sherr [5], the mirror level in ^{19}F has not been observed. Fortune and Sherr suggest that the Coulomb shift should be quite large, owing to the large spectroscopic factor. This is confirmed by our microscopic approach, which suggests its energy near $E_x = 7.9$ MeV (Fortune and Sherr propose $E_x = 7.4 \pm 0.1$ MeV). Such a large Coulomb shift is typical of s waves with a large reduced width [30].

From an experimental point of view, many $3/2^+$ states are known in ^{19}F up to 8 MeV. Although the cluster theory does reproduce three of them, some other states are missing. An obvious drawback of the model is that the $3/2^+$ doublets near 6.5 MeV cannot be described, although their states are very near the ^{18}F+p threshold in ^{19}Ne. This problem is well known in cluster models: it arises from the limited number of configurations. When a resonance is missing in the GCM, it should correspond to other cluster configurations, such as three-body structures or other two-body arrangements. This means that the ^{18}F+p and α+^{15}O configurations, included in the model, should play a minor role, and that the spectroscopic factors in these channels should be significantly lower than the values shown in Table 3. This argument is supported experimentally by the very small Coulomb shifts.

Concerning missing states, it is worth mentioning the experimental $3/2^+_2$ states at 3.91 MeV in ^{19}F and at 4.03 MeV in ^{19}Ne. These states are expected to determine the ^{15}N$(\alpha,\gamma)^{19}$F and ^{15}O$(\alpha,\gamma)^{19}$Ne reaction rates, as they are located near the α threshold. Previous α+^{15}N (α+^{15}O) cluster studies concluded that these states do not present an α structure and that, consequently, the reduced α widths should be quite small [29]. They are still missing here, although many additional channels are included. This result seems to support the suggestion of Ref. [29], i.e. that the missing $3/2^+$ states might belong to a band with a more deformed structure, such as ^{12}C+^{7}Li (^{12}C+^{7}Be).

A microscopic cluster model provides a unified description of bound and scattering states. The determination of the scattering wave function and of the collision matrix is performed within the R-matrix theory, which exactly accounts for boundary conditions. The transfer cross section from the proton to the α channel is defined as

$$\sigma_t(E) = \frac{\pi}{k^2} \sum_{J\pi} \frac{2J+1}{(2I_1+1)(2I_2+1)} \sum_{\ell\ell' II'} |U^{J\pi}_{p\ell I,\alpha\ell' I'}(E)|^2, \tag{6}$$

where $(I_1 = 1, I_2 = 1/2)$ are the spins of the colliding nuclei, $J\pi$ are the total spin and parity, and k is the wave number in the entrance channel. This definition is valid for resonant as well as for non-resonant processes, and only depends on the collision matrix $U^{J\pi}$. The transfer cross section is deduced from non-diagonal elements of the collision matrix: (ℓI) are the angular momentum and channel spin in the entrance channel, whereas $(\ell' I')$ are the corresponding values in the exit channel.

In the present calculation, only s-waves are included, which means that the summation over $J\pi$ in Eq. (6) is limited to $J\pi = 1/2^+$ and $3/2^+$. The first step is to determine the transfer cross section from the GCM wave functions. Then, as some states are missing or slightly shifted with respect to experiment, we will use the ability of the R-matrix theory to combine GCM results with experimental information.

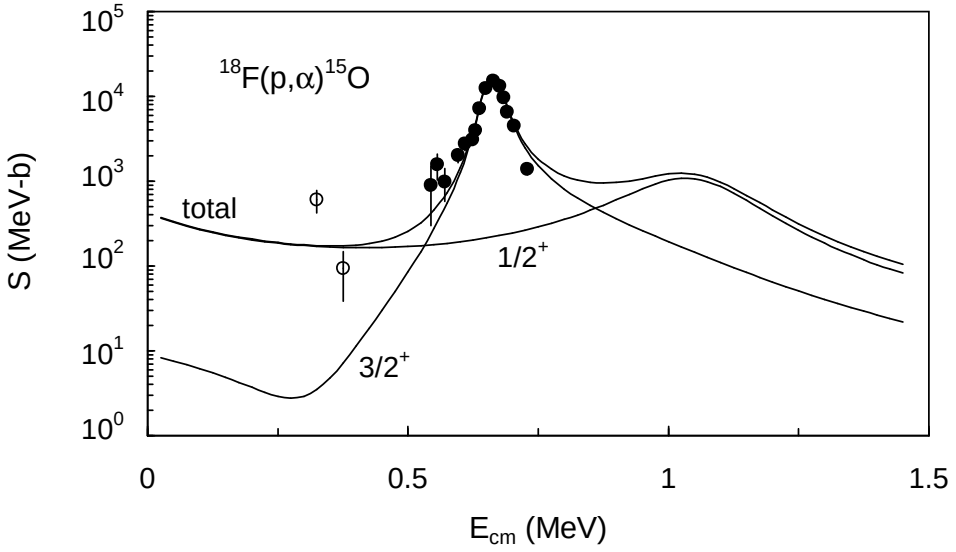

Fig. 3. ^{18}F(p,α)^{15}O S-factor for $J = 1/2^+$ and $J = 3/2^+$. The experimental data are taken from Ref. [9] (full circles) and Ref. [14] (open circles).

The GCM S-factor is shown in Fig. 3. Near the $3/2^+$ resonance, the agreement with the data is excellent, as only the energy has been fitted by the NN interaction. Below 0.3 MeV, the $3/2^+$ contribution presents an interference pattern, due to other $3/2^+$ resonances. The $1/2^+$ contribution is essentially determined by the properties of a broad resonance near 1 MeV, and of subthreshold state (see Fig. 1). One should of course keep in mind that some $3/2^+$ states are missing in the region 0-0.5 MeV, but our calculation suggests that the $1/2^+$ partial wave plays an important role.

This S-factor can be considered as a fair estimate, but some resonances are missing, and others are not located at the experimental energy. To improve the accuracy on the theoretical S-factor, we have combined GCM information with experimental data. This procedure has been successfully used in other reactions, such as ^{12}C$(\alpha,\gamma)^{16}$O for example [31]. Let us start with the $1/2^+$ contribution. As shown in Fig. 3, two states determine the S-factor. The microscopic calculation suggests that interference effects are negligible, and that the $1/2^+$ S-factor can be approximated by the sum of two isolated states. These states are known experimentally in ^{19}F, but are not observed in ^{19}Ne. It is reasonable to assume that the differences between the GCM and experimental energies are identical for the mirror nuclei. The ^{19}Ne energies have been therefore corrected by this difference, and the partial widths, unknown in ^{19}F, are modified according to the energy shift. The ^{19}Ne properties of these states are given in Table 5, and the two-level S-factor in Fig. 4. According to the previous discussion, interference effects have been neglected. Comparing with Fig. 3 provides a reduction of the $1/2^+$ contribution since the resonance is shifted upwards and the subthreshold state downwards.

Table 5
Spectroscopic properties (in MeV) of $1/2^+$ states in ^{19}Ne near the proton threshold.

E_{GCM}	E_{mod}	Γ_p	Γ_α
-0.15	-0.41	1.95×10^{-3} [a)]	0.231
1.11	1.49	0.157	0.139

[a)] Reduced width at 10.1 fm.

For the $3/2^+$ partial wave, a similar procedure has been used. We have complemented the microscopic R-matrix calculation with the two states of the doublet ($E_{cm} = 8$ keV and 38 keV). Partial widths have been taken from the literature [12]. As the interference signs are not known, we have considered the four possibilities. This procedure provides the different curves in Fig. 4. They correspond to the total S factor. In Ref. [4], the authors investigate

$3/2^+$ interference effects in an R-matrix analysis. Considering three $3/2^+$ levels, Chae *et al.* find that each of the 8 sign combinations gives a different χ^2. This conclusion is surprising since a common change of all signs should not modify the S-factor.

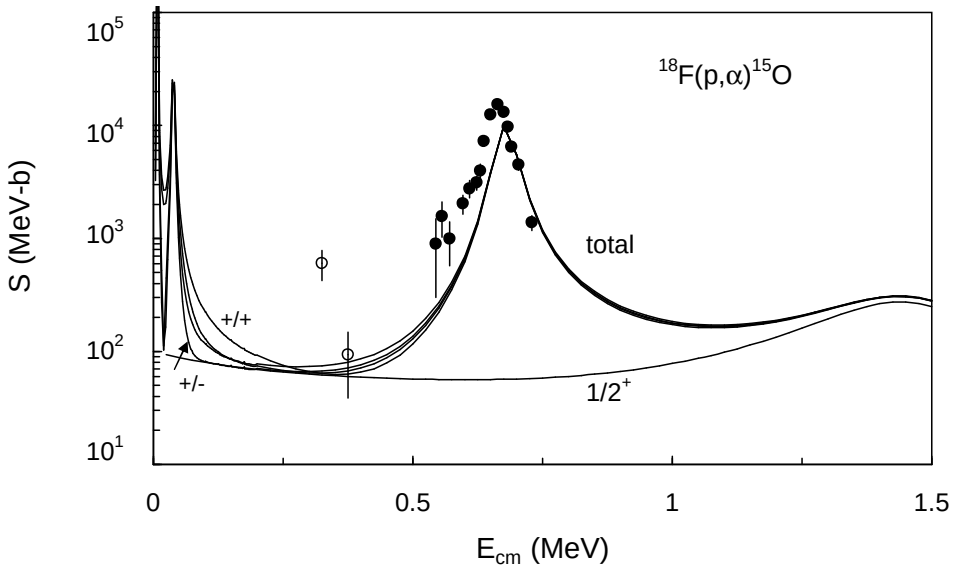

Fig. 4. Corrected ^{18}F(p,α)^{15}O S-factor, with the individual contribution of $J = 1/2^+$ (see text). The signs correspond to different interference signs in the $3/2^+$ partial wave. The data are as in Fig 3.

Within the resonance, Fig. 4 shows that the theory slightly underestimates the data. This could be compensated by a slight readjustment of the partial widths, but our goal here is a qualitative discussion, rather than an accurate fit of the data. The main conclusion from Fig. 4 is that, in the temperature range typical of novae (corresponding to $E_{cm} \approx 0.2 - 0.3$ MeV) the uncertainties of the S-factor due to the interference patterns is much smaller than expected [32]. The reason is that the main contribution at nova energies comes from the $1/2^+$ partial wave.

3.5 Discussion of $J = 1/2^+$ states

Currently, the relevant $1/2^+$ states are observed in ^{19}F, but have not been experimentally studied in ^{19}Ne. A spectrum of expected $1/2^+$ states in ^{19}Ne is displayed in Fig. 5. The known states are shown as solid thin lines, and the predicted levels (from Table 5) are shown as thick lines. The theoretical widths are given in Table 5. Experimental information about these resonances seems to be crucial for a good knowledge of the ^{18}F(p,α)^{15}O cross section at

novae temperatures.

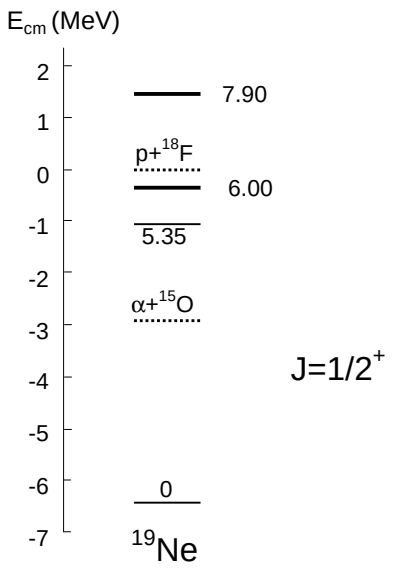

Fig. 5. Theoretical ^{19}Ne level scheme for $J = 1/2^+$. Thin levels are experimentally known, and the thick lines correspond to GCM energies corrected by the energy difference in ^{19}F.

The main novelty of this work deals with new $1/2^+$ states near the proton threshold in ^{19}Ne. Experimentally, the second state could be observed by elastic scattering. It is interesting to point out that, in a ^{18}F+p elastic-scattering experiment, Bardayan *et al.* [11] mention the need for a broad s state to fit their cross section. This experiment was however limited to energies $E_{cm} < 1.01$ MeV, and a clear identification could not be performed.

We present in Fig. 6 the theoretical scattering cross section at $\theta_{cm} = 180°$ (corresponding to $\theta_{lab} = 0°$ in reverse kinematics). This cross section should be considered as qualitative only, as only the $1/2^+$ and $3/2^+$ partial waves have been included (for other partial waves, up to $\ell = 2$, we use the hard-sphere approximation of the phase shift). The subtreshold $1/2^+$ state does not play any role near 1.5 MeV. Its contribution is limited to lower energies, where the Coulomb term dominates. Accordingly, the elastic cross section is not sensitive to its properties. The main emphasis should be put on the difference between the cross section with and without the broad $1/2^+$ state. Its presence provides a clear signature in the cross section, and should be observable in future experiments.

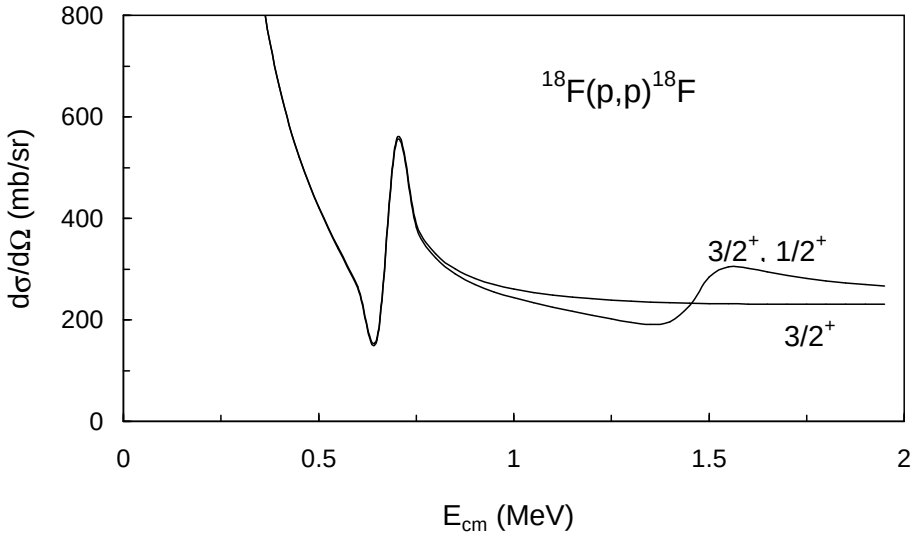

Fig. 6. ^{18}F+p elastic cross section at $\theta_{cm} = 180°$, with the $3/2^+$ partial wave only, and with the addition of $J = 1/2^+$.

4 Conclusion

This work is aimed at providing an exploring study of the ^{18}F(p,α)^{15}O reaction from a microscopic viewpoint. This approach cannot be expected to fit the experimental data but, instead, to give qualitative arguments about the energy spectra, cross sections, and other physical quantities. Consequently, it represents an ideal complement to fitting procedures, such as the phenomenological R-matrix method, which provides more accurate extrapolations, but necessarily requires cross-section or/and spectroscopic data.

The high number of channels included in the present GCM basis represents a challenge. As mentioned in Section 2, the basis involves 28 ^{18}F+p channels, 2 ^{15}O+α channels and 14 ^{18}Ne+n channels. This property allows us to span the *sd* shell. The main advantage of the GCM is to provide, in addition to spectroscopy, scattering wave functions of the system. This is crucial in low-energy reactions where the Coulomb interaction is dominant.

We have essentially focused on $1/2^+$ and $3/2^+$ states, i.e. s-waves in the ^{18}F+p system. Our nucleon-nucleon interaction is adjusted on the energy of the 7.07 MeV single-particle state in ^{19}Ne. All other quantities (resonance energies and widths, cross sections, etc) are obtained without any fitting. As expected for relatively high level densities, the GCM does not reproduce all ^{19}Ne experimental states. Missing states should have more complicated structures, such as three-body structures and, consequently, should be characterized by small ^{18}F+p spectroscopic factors. In particular the experimental $3/2^+$ doublets in ^{19}F and ^{19}Ne are not described by the model. In addition it is known (see, for example, Ref. [14]) that p waves should play a role.

Our main conclusion is that the $1/2^+$ partial wave plays an important role in the ^{18}F(p,α)^{15}O cross section. This is not surprising as it represents an s wave, but has been dismissed until now. Our model suggests that the $1/2^+$ contribution should essentially arise from a subthreshold state, and from a broad resonance near 1.4 MeV. In these conditions, the S-factor at typical novae temperatures (E_{cm} $0.2-0.3$ MeV) is dominated by the $1/2^+$ term, and the interference problem between $3/2^+$ resonances is reduced. Accordingly, if the properties of these $1/2^+$ states are confirmed, the uncertainties on the ^{18}F(p,α)^{15}O reaction rate should be lower than expected. From the energy and width, the 8.65 MeV level in ^{19}F is a very good candidate for the broad $1/2^+$ resonance. It is expected near 7.7 MeV in ^{19}Ne ($E_{cm} \approx 1.5$ MeV). The existence of a new s state at $E_{cm} > 1.01$ MeV is suggested by Bardayan *et al.* [11], and might correspond to the GCM state. From the theoretical point of view, this level can be considered as a single-particle state, with a structure very similar to the $3/2^+$ resonance at 7.07 MeV. An experimental confirmation of this $1/2^+$ state, with an elastic-scattering experiment, should provide an important step in a better understanding of the ^{18}F(p,α)^{15}O process.

Acknowledgements

We are grateful to Carmen Angulo and Nicolas de Séréville for helpful discussions. This text presents research results of the Belgian program P5/07 on interuniversity attraction poles initiated by the Belgian-state Federal Services for Scientific, Technical and Cultural Affairs.

References

[1] A. Coc, M. Hernanz, J. José, J.-P. Thibaud, Astron. Astrophys. 357 (2000) 561.

[2] M. Hernanz, J. Gómez-Gomar, J. José, New Astronomy Review 46 (2002) 559.

[3] D.R. Tilley, H.R. Weller, C.M. Cheves, R.M. Chasteler, Nucl. Phys. A 595 (1995) 1.

[4] K.Y. Chae, D.W. Bardayan, J.C. Blackmon, D. Gregory, M.W. Guidry, M.S. Johnson, R.L. Kozub, R.J. Livesay, Z. Ma, C.D. Nesaraja, S.D. Pain, S. Paulauskas, M. Porter-Peden, J.F. Shriner Jr., N. Smith, M.S. Smith, J.S. Thomas, Phys. Rev. C 74 (2006) 012801.

[5] H.T. Fortune, R. Sherr, Phys. Rev. C 61 (2000) 024313.

[6] H.T. Fortune, R. Sherr, Phys. Rev. C 73 (2006) 024302.

[7] R. Coszach, M. Cogneau, C. R. Bain, F. Binon, T. Davinson, P. Decrock, Th. Delbar, M. Gaelens, W. Galster, J. Görres, J.-S. Graulich, R. Irvine, D. Labar, P. Leleux, M. Loiselet, C. Michotte, R. Neal, G. Ryckewaert, A.S. Shotter, J. Vanhorenbeeck, J. Vervier, M. Wiescher, Ph. Woods, Phys. Lett. B 353 (1995) 184.

[8] J.-S. Graulich, F. Binon, W. Bradfield-Smith, M. Cogneau, R. Coszach, T. Davinson, Th. Delbar, M. Gaelens, W. Galster, J. Görres, D. Labar, P. Leleux, M. Loiselet, J. McKenzie, R. Neal, G. Ryckewaert, A.C. Shotter, J. Vanhorenbeeck, J. Vervier, M. Wiescher, Ph. Woods, Nucl. Phys. A 626 (1997) 751.

[9] D.W. Bardayan, J.C. Blackmon, W. Bradfield-Smith, C.R. Brune, A.E. Champagne, T. Davinson, B.A. Johnson, R.L. Kozub, C.S. Lee, R. Lewis, P.D. Parker, A.C. Shotter, M.S. Smith, D.W. Visser, P.J. Woods, Phys. Rev. C 63 (2001) 065802.

[10] J.-S. Graulich, S. Cherubini, R. Coszach, S. El Hajjami, W. Galster, P. Leleux, W. Bradfield-Smith, T. Davinson, A. Di Pietro, A.C. Shotter, J. Görres, M. Wiescher, F. Binon, J. Vanhorenbeeck, Phys. Rev. C 63 (2001) 011302.

[11] D.W. Bardayan, J.C. Blackmon, J.Gomez del Campo, R.L. Kozub, J.F. Liang, Z. Ma, L. Sahin, D. Shapira, M.S. Smith, Phys. Rev. C 70 (2004) 015804.

[12] S. Utku, J.G. Ross, N.P.T. Bateman, D.W. Bardayan, A.A. Chen, J. Gorres, A.J. Howard, C. Iliadis, P.D. Parker, M.S. Smith, R.B. Vogelaar, M. Wiescher, K. Yildiz, Phys. Rev. C 57 (1998) 2731, Erratum Phys. Rev. C 58, 1354 (1998).

[13] Y.M. Butt, J.W. Hammer, M. Jaeger, R. Kunz, A. Mayer, P.D. Parker, R. Schreiter, G. Staudt, Phys. Rev. C 58 (1998) R10.

[14] D.W. Bardayan, J.C. Batchelder, J.C. Blackmon, A.E. Champagne, T. Davinson, R. Fitzgerald, W.R. Hix, C. Iliadis, R.L. Kozub, Z. Ma, S. Parete-Koon, P.D. Parker, N. Shu, M.S. Smith, P.J. Woods, Phys. Rev. Lett. 89 (2002) 262501.

[15] N. de Séréville, A. Coc, C. Angulo, M. Assuncaõ, D. Beaumel, B. Bouzid, S. Cherubini, M. Couder, P. Demaret, F. de Oliveira Santos, P. Figuera, S. Fortier, M. Gaelens, F. Hammache, J. Kiener, D. Labar, A. Lefebvre, P. Leleux, M. Loiselet, A. Ninane, S. Ouichaoui, G. Ryckewaert, N. Smirnova, V. Tatischeff, J.P. Thibaud, Phys. Rev. C 67 (2003) 052801.

[16] R.L. Kozub, D.W. Bardayan, J.C. Batchelder, J.C. Blackmon, C.R. Brune, A.E. Champagne, J.A. Cizewski, T. Davinson, U. Greife, C.J. Gross, C.C. Jewett, R.J. Livesay, Z. Ma, B.H. Moazen, C.D. Nesaraja, L. Sahin, J.P. Scott, D. Shapira, M.S. Smith, J.S. Thomas, P.J. Woods, Phys. Rev. C 71 (2005) 032801.

[17] D.W. Bardayan, R. L. Kozub, M.S. Smith, Phys. Rev. C 71 (2005) 0188801.

[18] R.L. Kozub, D.W. Bardayan, J.C. Batchelder, J.C. Blackmon, C.R. Brune, A.E. Champagne, J.A. Cizewski, U. Greife, C.J. Gross, C.C. Jewett, R.J. Livesay, Z. Ma, B.H. Moazen, C.D. Nesaraja, L. Sahin, J.P. Scott, D. Shapira, M.S. Smith, J.S. Thomas, Phys. Rev. C 73 (2006) 044307.

[19] M. Dufour, P. Descouvemont, Nucl. Phys. A 750 (2005) 218.

[20] M. Dufour, P. Descouvemont, Phys. Rev. C 72 (2005) 015801.

[21] K. Wildermuth, Y.C. Tang, "A Unified Theory of the Nucleus", ed. by K. Wildermuth and P. Kramer, Vieweg, Braunschweig (1977).

[22] D. Baye, P.-H. Heenen, M. Libert-Heinemann, Nucl. Phys. A 291 (1977) 230.

[23] S. Saito, S. Okai, R. Tamagaki, M. Yasuno, Prog. Theor. Phys. 50 (1973) 1561.

[24] T. Fliessbach, H. Walliser, Nucl. Phys. A 377 (1982) 84.

[25] K. Varga, R.G. Lovas, Phys. Rev. C 37 (1988) 2906.

[26] C. Iliadis, M. Wiescher, Phys. Rev. C 69 (2004) 064305.

[27] D. Baye and N. Pecher, Bull. Cl. Sc. Acad. Roy. Belg. 67 (1981) 835.

[28] T. Sakuda, F. Nemoto, Prog. Theor. Phys. 62 (1979) 1274; Prog. Theor. Phys. 62 (1979) 1606.

[29] P. Descouvemont, D. Baye, Nucl. Phys. A 463 (1987) 629.

[30] C. Angulo, G. Tabacaru, M. Couder, M. Gaelens, P. Leleux, A. Ninane, F. Vanderbist, T. Davinson, P.J. Woods, J.S. Schweitzer, N.L. Achouri, J.C. Angélique, E. Berthoumieux, F. De Oliveira Santos, P. Himpe, P. Descouvemont, Phys. Rev. C 67 (2003) 014308.

[31] P. Descouvemont, D. Baye, Phys. Rev. C 36 (1987) 1249.

[32] N. de Séréville, E. Berthoumieux, A. Coc, Nucl. Phys. A 758 (2005) 745c.